Journal of Shipping and Ocean Engineering 11 (2021) 53-63
Doi:10.17265/2159-5879/2021.02.001

# Saco-Casco Bays Inundation Modeling of Five Winter Storms

Saswati Deb[1], Huijie Xue[2], and Shivanesh Rao[3]

*1. Fisheries and Oceans Canada, Gulf Fisheries Centre, New Brunswick, Canada*

*2. School of Marine Sciences, University of Maine, Maine, USA*

*3. School of Physical, Environmental and Mathematical Sciences, University of New South Wales, Canberra, Australia*

**Abstract:** Coastal inundation along the northeast coast of the United States is usually caused by strong winter storms (WS). However, the accurate prediction of coastal inundation due to the WS is challenging. Therefore, our study aims to develop a unique high-resolution modeling system to accurately predict the coastal inundation in the ungauged coastal areas of Saco-Casco Bays and map the flood risk zones to potential sea level rise due to these storms. Hindcasts of five classic WS in 2014-2015 were studied. The inundation models are based on FVCOM that uses unstructured grid to capture the minor to significant flooding near the shallow areas of the bays, harbor entrance and river banks. In this study, topography has been generated from the NOAA's integrated dataset of Portland, ME 1/3 arc-second MHW digital elevation model. The model runs were driven by two different sets of meteorological (NECOFS WRF and NOAA's NAM WRF) forcing to examine the effect of spatial resolution on the predicted inundation. The study reveals that among the five storm surge cases, WS-III produces a maximum surge of 0.7 m and WS-II cause a minimum surge of 0.3 m. In all scenarios, southward wind-driven coastal current flowing towards Biddeford Pool, Pine Point and Camp Ellis forms a small-scale eddy which causes significant inundation however strength of the current varies accordingly. Sensitivity experiments have been carried out using NECOFS WRF simulation products with varying parameters of marshland elevation and bottom friction to understand the influence of intertidal storage on the predicted flooding.

**Key words:** Coastal inundation, winter storms, Saco-Casco Bays, FVCOM, NECOFS WRF.

## 1. Introduction

Storm surges due to wintertime extra-tropical cyclones typically known as nor'easters or winter storms (WS) are pretty common along the northeast coast of United States. Each year these storms cause significant inundation along the coastal areas of the Gulf of Maine (GOM) with damages to property and loss of life [1, 2]. Yet, accurate prediction of coastal inundation due to the WS is difficult due to variety of reasons. The key factors that regulate the storm surges caused due to these wintertime extra-tropical cyclones are (i) low pressure system, (ii) wind setup, (iii) high astronomical tide (iv) wave run up and (v) heavy precipitation [3, 4]. Among these factors, the low-pressure system and wind set-up along with high astronomical tide mostly influence the surge level at the open coast of the bay.

The long sandy arcuate shoreline of Saco Bay is one of the notable areas of GOM, which is prone to storm-induced erosion and coastal flooding [5, 6]. Therefore, our study focused on five classic winter storms of 2014-15, which impacted the southern Maine coastal region and caused minor to significant flooding near the low-lying areas of the Saco-Casco Bays, harbor entrance and along the river banks. These onshore surges and water level elevation are also influenced by the bathymetry and coastline as shallow depth in Saco Bay are likely to produce higher surges compared to steeper slopes of Casco Bay.

In order to improve the prediction capability of the coastal flooding along the east coast of U.S., different storm surge modeling studies were conducted [7, 8].

**Corresponding author:** Saswati Deb, Ph.D.; research fields: physical and biological oceanographer. E-mail: saswati.deb@dfo-mpo.gc.ca.

These studies suggested that the inclusion of high resolution model grid could potentially improve the prediction skill of coastal inundation. However, accurate prediction of inundation along the coastal areas of Saco Bay is challenging due to non-availability of tide gauge (TG) stations. On the other hand, Casco Bay includes one TG station located at Portland (station number ME8418150) that provides both predicted and verified water level observations. So, our study area (Fig. 1a) extends from Saco Bay in the south to Casco Bay in the north. In Saco Bay, tides are only predicted based on harmonic constants at Pine Point, Old Orchard Beach, and Camp Ellis areas, but without the actual sea level measurements. It is therefore hard to accurately determine the storm surges in these frequent flooding zones. To aid with the analysis, the University of Maine, was funded by the Cooperative Institute for the North Atlantic Region (CINAR) of NOAA, to deploy a mooring in Saco Bay (ME198) during the fall of 2014.

Therefore, our study aims to develop a unique high-resolution modeling framework based on unstructured grid finite-volume method to accurately predict the coastal inundation and map the flood risk zones to potential sea level rise due to these wintertime extra-tropical storms in ungauged low-lying coastal areas of Saco-Casco Bays. The model runs were driven by two different sets of meteorological forcing, Northeast Coastal Ocean Forecast System Weather Research and Forecasting Model (NECOFS WRF; ~9 km resolution) and North American Mesoscale (NOAA's NAM; 218 AWIPS Grid ~12 km resolution) Weather Research and Forecasting Model, in two separate simulations to examine the effect of spatial resolution on predicted inundation. Further, sensitivity experiments are performed with varying parameters of marshland elevation and bottom friction to understand the effect of intertidal storage on the predicted flooding.

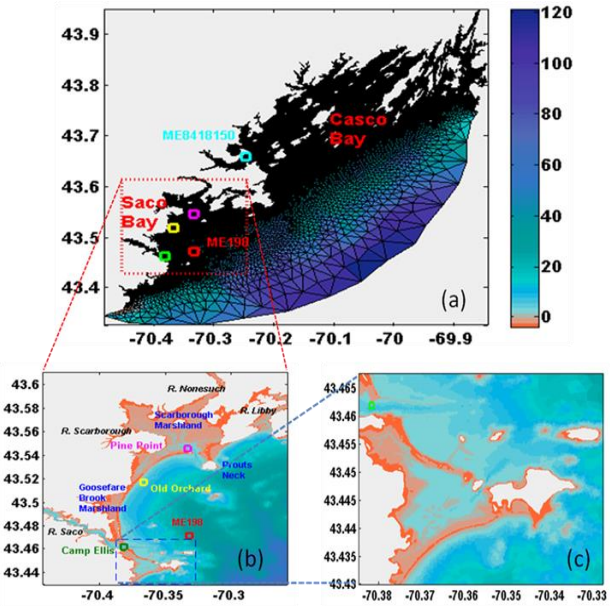


**Fig.1 Map showing (a) Saco-Casco Bays model grid and bathymetry in meters, (b) zoomed in to the Saco Bay. Color squares represent several key locations (magenta: Pine Point; yellow: Old Orchard Beach; green: Camp Ellis; red: buoy ME198) where water levels are extracted from the model for analysis; and (c) further zoomed in to the Biddeford Pool area.**

## 2. Data, Model, and Methodology

### *2.1 The Saco-Casco Bays Inundation Model*

The three-dimensional Saco-Casco Bays inundation model is based on finite-volume coastal ocean model (FVCOM) and includes tidally driven flooding and drying of intertidal areas [9]. The model is characterized by unstructured triangular grids in the horizontal and terrain–following coordinate in the vertical. The horizontal mixing is based on the Smagorinsky turbulence scheme [10], and the vertical mixing is calculated using Mellor and Yamada level 2.5 [11]. The model resolves the integral form of the governing equations by second-order, flux-based, finite-volume schemes [12]. The Saco-Casco Bays model bathymetry is generated from the Portland, ME 1/3 arc-second mean high water (MHW) digital elevation model (DEM), which was built in December 2008 to support NOAA's Tsunami Program [13]. Each cell size of the DEM is ~10 m and the vertical datum is referenced to MHW. The model grid varying from ~9 m near the shallow coastal areas to ~6 km at the open boundary is chosen for our study, which results in a total of 303042 nodes and 578975

elements (Fig. 1a). The model has 20 sigma levels in the vertical, which follows the parabolic function as shown in Eq (1).

$$\sigma(k) = [(k-1)/(kb-1)]^{P\_Sigma} \quad (1)$$

Here $k$ is equal to 1, 2, …, $kb$. The $kb$ is total number of sigma levels. To allow higher resolution near the surface and bottom, we considered *P_Sigma* is equal to 2. The Saco-Casco Bays inundation models are one-way nested with the NECOFS-GOM3. The NECOFS-GOM3 coastal inundation model is an integrated surface wave/atmosphere/coastal ocean modeling system designed for monitoring the coastal flooding in northeast U.S. regions [8]. The products derived from NECOFS-GOM3 are of coarser resolution. These derived products are used as initial and boundary conditions in the model. River Saco in Saco Bay and River Presumpscot in Casco Bay, add fresh-water input into the model. These daily discharge rates are based on United States Geological Survey (USGS) data. Then, these models are driven by two discrete set of three hourly meteorological forcing. One with moderate resolution NAM WRF represented as MNAM and another with NECOFS WRF denoted as MNEC in two separate simulations.

We used a simple algorithm [14] to compute the drag coefficient from the wind speed:

$$\begin{gathered} C_{D,LP} = 1.2\times10^{-3}, \\ for\ 4 \le \overline{V} < 11 ms^{-1} \\ C_{D,LP} = (0.49 + 0.065\overline{V})\times10^{-3} \\ for\ \ 11 \le \overline{V} \le 25 ms^{-1} \end{gathered} \quad (2)$$

where $\overline{V}$ is the absolute value of the wind speed, and $C_{D,LP}$ denotes the drag coefficient.

In these inundation models, the bottom frictional stress is calculated using the quadratic formula:

$$\left(\tau_x, \tau_y\right) = \rho \times C_d \times \sqrt{u^2 + v^2} \times (u, v) \quad (3)$$

where, $\tau_x$ and $\tau_y$ are bottom shear stress in the $x$ and $y$ directions, and $\rho$ is the water density. The velocities in x and y directions are represented as u and $v$, respectively. $C_d$ is the drag coefficient calculated as a log function of the bottom layer thickness, $Z_{bl}$.

$$C_d = \max\left[\left(\kappa / \ln\left(\frac{Z_{bl}}{Z_0}\right)\right)^2, fric\right] \quad (4)$$

Here, $\kappa$ =0.4 is the von Karman constant and $Z_0$=0.001 is the bottom roughness. A varying parameter denoted as *fric*, is the frictional coefficient in deep water.

### *2.2 Case Studies of Five Winter Storms*

Our study focused on the five typical WS of 2014-2015 and the detailed storm tracked path based on NECOFS WRF are depicted in Fig. 2. The WS-I smashed the coast of New England around 15:00 GMT on October 23, 2014 with a low-pressure system of ~995 mb centered approximately at 39.63°N and 72.7°W. The big and slow moving WS-II arrived on early morning of 2 November, 2014. NECOFS WRF showed that a low-pressure system of 996 mb was initially centered around 38.89°N and 69.09°W at 23:00 GMT on 1 November, 2014 but further dropped to ~985 mb at 15:00 GMT on November 2, 2014 and caused flooding along the coast of Saco-Casco Bays. The WS-III arrived on 26 January, 2015 at 23:00 GMT with a low-pressure system of996 mb. Then, the pressure started to drop at the rate of 1.5 mb per hour in the next few hours with increased wind speed. It caused a maximum inundation along the coast of Saco-Casco Bays at 9:00 GMT on 27 January 2015. The WS-IV arrived late night of 14 February 2015. The low-pressure system dropped to 975 mb at 12:00 GMT on 15 February with increased speed of northeast winds and caused moderate flooding along the coast of the bays. Just on the heels of WS-IV, another WS-V arrived on early 19 February with a centered pressure of 996 mb approximately at 64.92°W and 38.9°N around 1:00 GMT on 19 February and caused maximum inundation at 3:00 GMT on the same day.

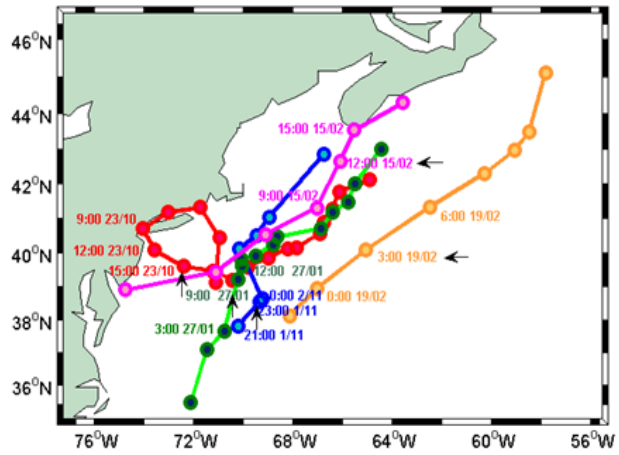


**Fig. 2 Storm track information for the five winter storms (WS) depicted from NECOFS WRF. Red, blue, green, magenta, orange line tracks WS-I, WS-II, WS-III, WS-IV and WS-V respectively. Black arrow represents the occurrence of storm-induced surge.**

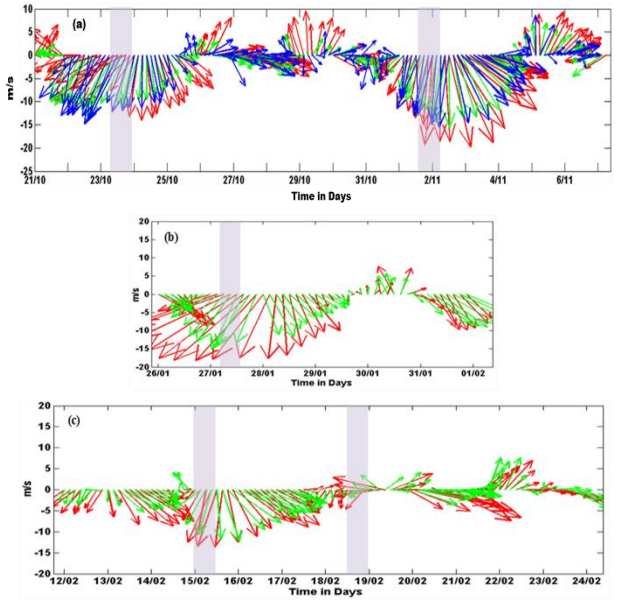


**Fig. 3 Comparison of vector wind plot for the five winter storms. (a) Vector wind of CINAR storm buoy, NECOFS WRF and NAM WRF are compared at ME198 for the WS-I and WS-II; (b) whereas vector wind of NECOFS WRF and NAM WRF are compared at ME8418150 for the WS-III, (c) WS-IV and WS-V. Time series of CINAR storm buoy, NECOFS WRF and NAM WRF vector wind are plotted in blue, red and green respectively. Peak storm surge period for the five winter storms are shaded.**

### *2.3 Wind Speed Comparisons*

The CINAR storm buoy, ME198 was deployed at 70.33218°W and 43.47129°N along the storm track to collect the real-time data of wind speed, wave height, water elevation, and other oceanographic parameters from 21 October, 2014 to December 3, 2014. Vector wind of NECOFS WRF and NAM WRF are compared with observed CINAR storm buoy (Fig. 3a) for the WS-I and WS-II. During all the storm events, the wind blew from NE and its magnitude of the speed gradually increased with the formation of low pressure system. Compared with the buoy data at ME198, both the wind speed and direction of NECOFS WRF showed slight deviation in case of WS-I. However, the hindcast results of wind speed and direction of NECOFS WRF well imitated in case of WS-II but slightly overestimated the peak wind speed compared to the buoy data. On the other hand, the NAM predicted wind showed good agreement with the buoy observations in both the storm cases with slightly underestimated peak speed. In case of WS-III (Fig. 3b), both NECOFS and NAM WRF showed that the northeast strong winds prevailed during the peak period. The wind directions changes rapidly in case of WS-IV and WS-V (Fig. 3c) however, storm surges were observed only when the winds blew from the northeast.

## 3. Results and Discussion

### *3.1 Comparison of Modeled Water Elevation with the Observations*

The inundation modeled (MNEC and MNAM) water elevation data are compared with the NOAA's verified water level at ME8418150 (location is shown in Fig 1a). This TG station is located in Casco Bay which provides both verified and predicted water levels. The predicted water levels are calculated based on harmonic analysis method, hence represent water levels associated with the astronomical tides whereas the verified values are the observed values. As there are no TG stations located in Saco Bay, therefore, model calibration in this bay was done by comparing the modeled dynamic height measurements (which includes both water elevation and water depth) with the observed values of CINAR storm buoy at ME198 (location is shown in Fig. 1b) for the first two winter storms.

The model-data comparison at ME8418150 and ME198 are detailed in Table 1. The surges estimated for the five storm events revealed that WS-III produces a maximum surge of 0.7 m and WS-II cause a minimum surge of 0.3 m. The estimation error of model simulated output are represented as over (+) or under (-) in comparison to the observed values. Both MNEC and MNAM underestimate the rise in water level at the peak of WS-I storm, around 15:00 GMT 23 October 2014 when compared with the observed water level at ME 8418150 by 31 cm and 33 cm respectively in amplitude with a same phase difference of ~15 min (Fig. 4a). However, these estimation errors in amplitudes and phases gets reduced for rest of the storm surge cases which is likely due to the improvement in the hindcast forcing field. As a whole, comparing the MNAM and MNEC simulated water levels with the TG verified data for all the storm surge scenarios, revealed that MNEC simulated water level produces results slightly better than MNAM. These slight differences in estimation of the peak tidal height during the passage of storm event indicates the importance of spatial resolution of the atmospheric forcing in better prediction of inundation. Further, statistical analysis of the model performance was employed based on root-mean-square-error (RMSE) between model and observed data. The RMSE is slightly higher in case of WS-I (28 cm) while minimum RMSE (12 cm) was noted in case of WS-IV (Table 3).

**Table 1 Model comparison with NOAA's water level at ME8418150 (43° 39.4' N and 70° 14.8' W).**

| Storm Surge Cases | Time Period | TG Predicted (meters) | TG Verified (meters) | Surge (meters) | MNEC (Meters) | MNAM (Meters) | MNEC – TG Verified (meters) | MNAM – TG Verified (meters) |
|---|---|---|---|---|---|---|---|---|
| WS-I | 23 Oct'14 15:00 GMT | 1.48 | 1.9 | 0.42 | 1.59 | 1.57 | -0.31 | -0.33 |
| WS-II | 1 Nov'14 23:00 GMT | 1.5 | 1.8 | 0.3 | 1.62 | 1.60 | -0.18 | -0.2 |
| WS-III | 27 Jan'15 9:00 GMT | 1.5 | 2.2 | 0.7 | 2.14 | 2.11 | -0.06 | -0.09 |
| WS-IV | 15 Feb'15 12:00 GMT | 1.4 | 1.9 | 0.5 | 1.91 | 1.89 | +0.01 | -0.01 |
| WS-V | 19 Feb'15 3:00 GMT | 1.6 | 2.0 | 0.4 | 1.90 | 1.88 | -0.10 | -0.12 |

**Table 2 Model comparison with CINAR Storm Buoy at ME198 (43.471 °N and 70.332 °W).**

| Storm Surge Cases | Time Period | Buoy (ME198) Dynamic Height (Meters) | MNEC (Meters) | MNEC-Buoy (Meters) |
|---|---|---|---|---|
| WS-I | 23 Oct'14 15:00 GMT | 26.42 | 26.57 | +0.15 |
| WS-II | 1 Nov'14 23:00 GMT | 26.54 | 26.71 | +0.17 |

**Table 3 RMSE analysis for the five storms surge events.**

| Storm Surge Cases | TG Verified vs TG Predicted (Meters) | TG Verified vs MNEC (Meters) | MNEC vs MNAM (Meters) |
|---|---|---|---|
| WS-I | 0.24 | 0.28 | 0.02 |
| WS-II | 0.18 | 0.19 | 0.01 |
| WS-III | 0.29 | 0.22 | 0.01 |
| WS-IV | 0.25 | 0.12 | 0.01 |
| WS-V | 0.20 | 0.17 | 0.01 |

We also validated the dynamic height of MNEC model with the real-time data of CINAR storm buoy (Fig. 5) in Saco Bay (Table 2). The dynamic height comparison revealed that the model overestimates the peak tidal height by 15 cm (Fig. 4b) and 17 cm with a same phase difference of ~20 min during the peak

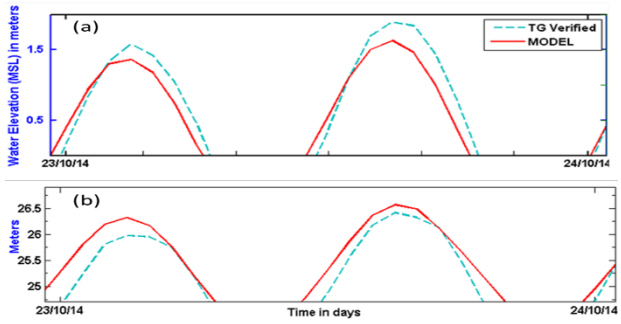


**Fig. 4 Water elevation are compared between the observations and model (MNEC) during the peak of WS-I (a) at ME 8418150 (Casco Bay) and (b) at ME198 (Saco Bay). Solid red line represents model and blue dashed line corresponds to NOAA's verified water level (TG) in the upper panel and CINAR storm buoy dynamic height in the bottom panel.**

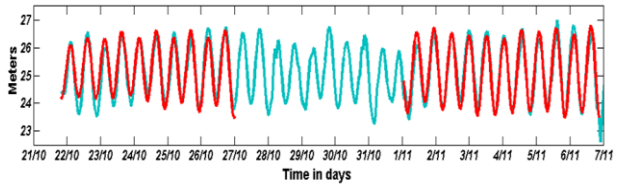


**Fig. 5 Model simulated dynamic height is compared with the CINAR storm buoy at ME198 for the two winter storms (WS-I and WS-II). Red and cyan colored line represents the model and buoy dynamic height respectively.**

of WS-I and WS-II respectively. In general, these demonstrates the capability of the model to timely and efficiently predict the rise in water level during the passage of extreme events. Therefore, MNEC can be used as a tool for storm surge forecasting in future. However, the small discrepancies observed between the model and buoy data are mainly due to the effect of different forcing fields, datum difference or due to varying composite phase of the tidal constituents.

We also compared the trend of surge between the two bays. Left panel of Fig. 6 represents the water elevation comparison between the NOAA's observed values with the harmonic analyzed values at ME 8418150 of Casco Bay for the five storm surge cases. Whereas mid panel of Fig. 6 showed comparison of MNEC water elevation with its harmonic constants at ME8418606 (ungauged Camp Ellis station) of Saco Bay. The storm-induced surge calculated for both Casco and Saco Bay are compared in the right panel of Fig. 6. The trend comparison revealed that the MNEC model is capable of predicting surges in the ungauged areas of Saco Bay. Overall, these results suggest that the MNEC model can be used as a tool to predict water elevation in the ungauged areas of Saco Bay and map the flood risk zones of the bay. Moreover, the spatial distribution of modeled water elevation during the pre-storm, peak-storm and post-storm period are compared with the normal tidal condition (Fig. 7) at the Biddeford Pool area of Saco Bay (location is shown in Fig. 1c). The figure shows that these areas are prone to frequent coastal flooding. The model is also capable of expounding the timing, and inundated areas at the Biddeford Pool during the passage of WS-I.

### *3.2 Model Simulated Currents*

During the peak of surge in all storm scenarios, the nearshore currents flowing from northeast, hits the low-lying areas of Biddeford Pool (43.452°N and 70.347°W) close to harbor entrance and forms the first stagnation point (Fig. 8a) in the southeastern head of the Saco Bay. This stagnation point is created due to the convergence of bi-directional currents and also due to local topographic effect of the region. The stagnation point separates these nearshore currents into two streams, one stream is directed towards southeast and another stream flow towards southwest to enter the Biddeford Pool with a speed greater than 1 m/s at the mouth of the harbor entrance causing significant inundation in these areas. The southward wind driven coastal current also hit the Camp Ellis point as it entered through the channel of Saco River. Subsequently discharge from the river formed a cyclonic eddy (43.4635°N and 70.379°W) at the harbor front. In all the storm surge cases, this cyclonic eddy is generated however the strength and shape of this eddy varies according to the storm-induced current velocity. This eddy directed flow caused substantial inundation along the banks of the Saco River. On the other hand, the strong currents flowing

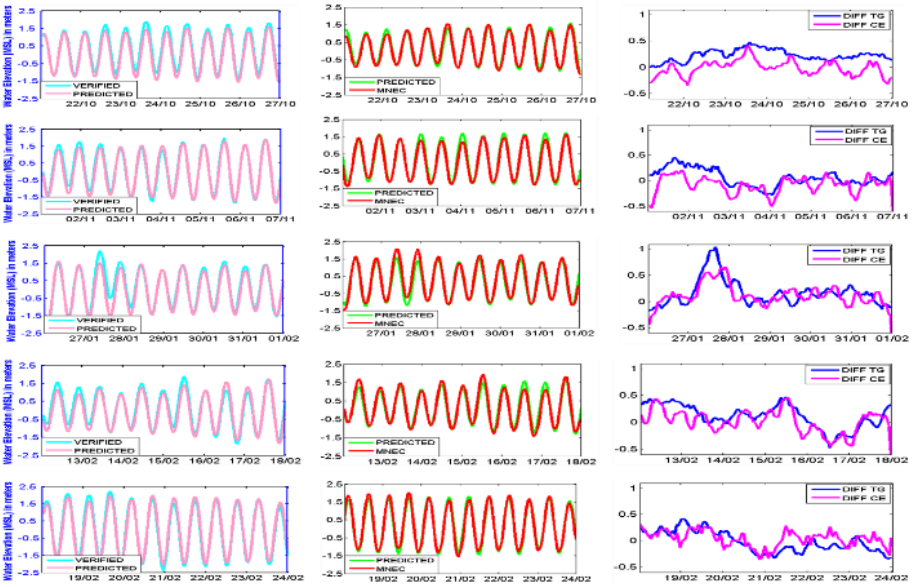


**Fig. 6 Comparison of water elevation for the five winter storms. Left panel represents water level comparison between the verified (observed) and predicted (harmonic analyzed) values at ME8418150 (TG of Casco Bay). Mid Panel compares the harmonic analyzed values with MNEC at ME8418606 (CE of Saco Bay). Right panel compares the trend from the differences.**

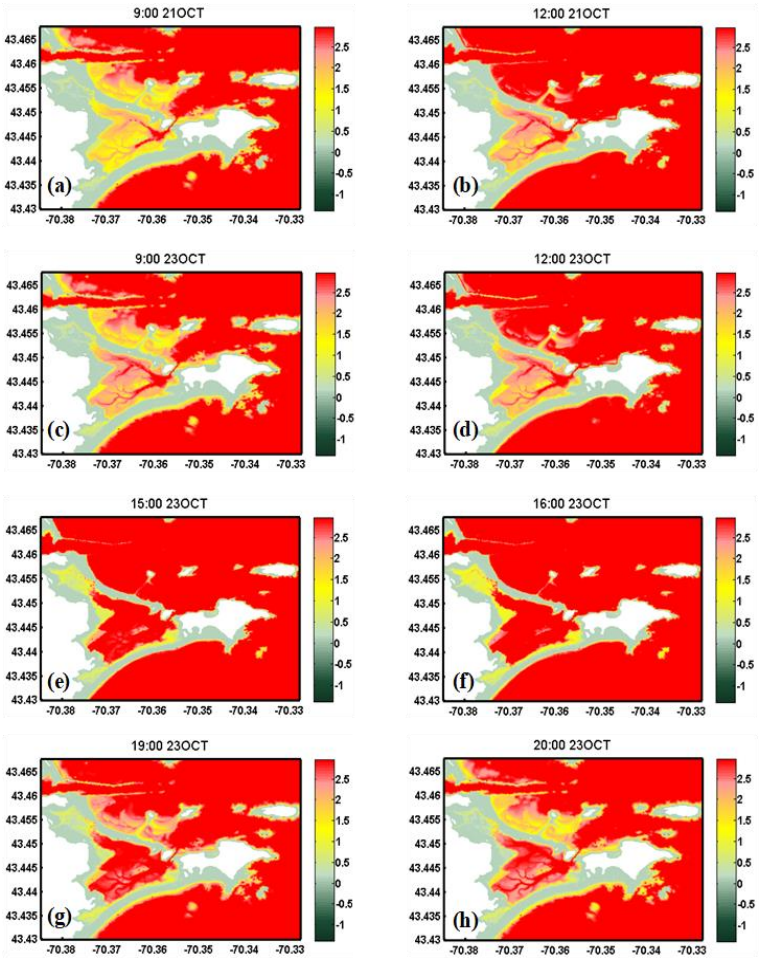


**Fig. 7 Spatial distribution of model simulated water elevation at Biddeford Pool area during the normal tide period (a and b); pre-storm period (c and d); peak-storm period (e and f); post-storm period (g and h).**

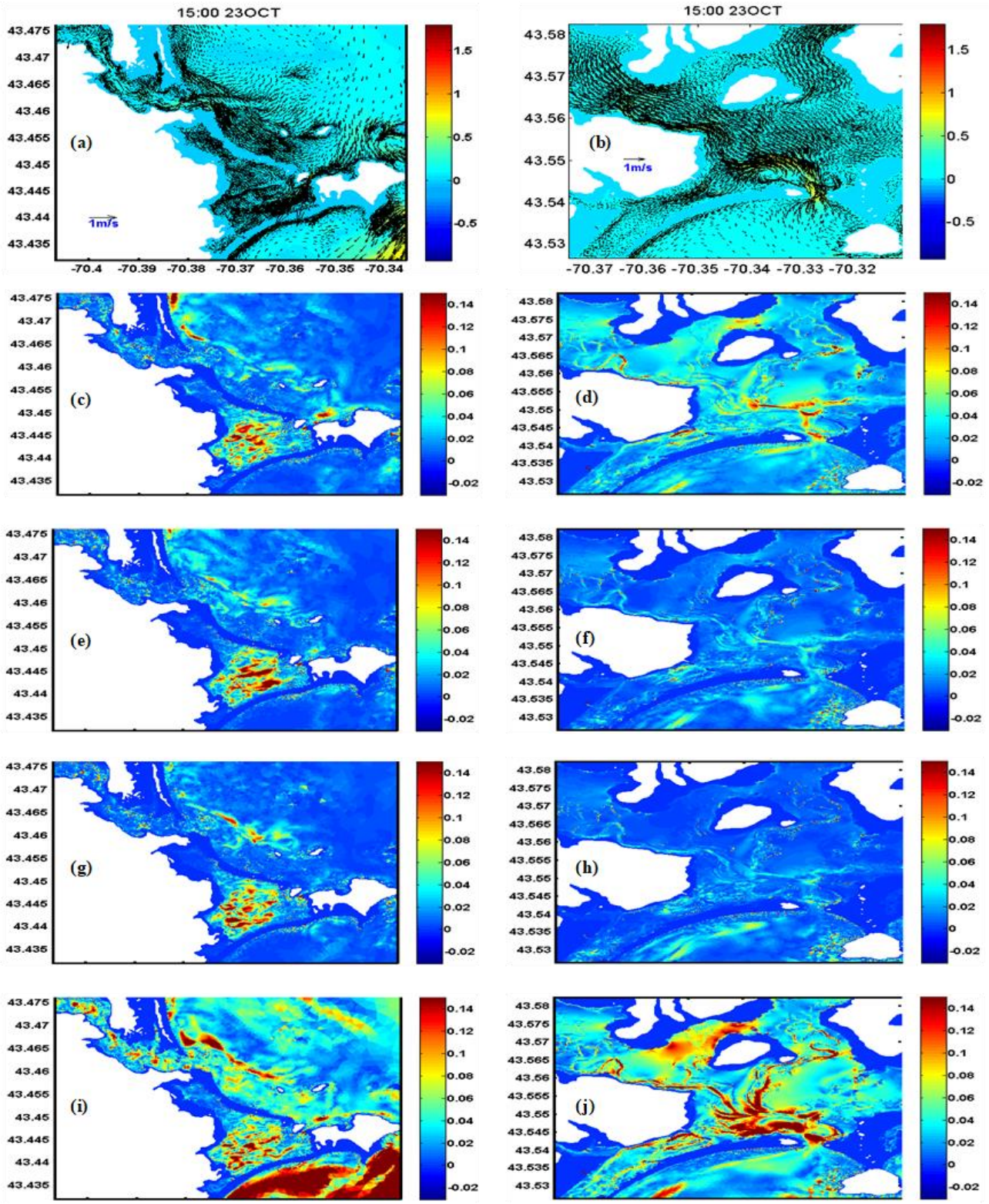


**Fig. 8 Spatial distribution of MNEC (CR) simulated surface currents in m/s for WS-I at 15 GMT on 23rd October 2014 are plotted for (a) south (left panel) and (b) north Saco Bay (right panel). For each sensitivity experiments, deviation in currents for during the peak storm are calculated as CR minus Exp-1 (c and d); CR minus Exp-2 (e and f); CR minus Exp-3 (g and h); CR minus Exp-4 (i and j).**

from northeast also hit the marshy areas of Pine Point in the northern head of the Saco Bay. The speed of the currents gets accelerated to almost 0.7 m/s (in WS-I) at the mouth of the Pine Point entrance and formed two separate cyclonic and anticyclonic eddies (Fig. 8b). Indeed, due to backflow and sand-clogged channels, these eddies are formed at the Pine Point harbor entrance in all storm scenarios. However, the strength and shape of these eddies varies depending on the strength/intensity of the intruding currents. The MNEC model showed that the maximum strength of the currents was 1.5 m/s in case of WS-III. These anticyclonic (centered at 43.544N and 70.324W) and cyclonic (centered at 43.5454°N and 70.336°W) eddies become stronger the next hour after the storm passage. Then these strong cyclonic eddy directed flow hits the marshy areas of Scarborough forming another stagnation point (43.5484°N and 70.3457°W). The position of this stagnation point seems to be confined due to the local effect of bathymetry and segregates the mainstream flowing from Pine Point into two directions. Major portion of the flow headed northwards in marshy areas of Scarborough with accelerated speed causing inundation along the banks of the Scarborough river. However, as the stream heads further northward the strength of current gets reduced due to strong bottom friction induced by marshland. Another flow that head towards west of Pine Point caused a mild to moderate inundation.

Our study is the first attempt to provide detailed information of the flow pattern in the north and south of Saco Bay. The study suggests that the main difference in the variation of surges among all these wintertime inundation cases is the storm-induced strength in current velocity which influences the extent of the inundation. However, the strength of these currents flowing from northeast depends on wind speed and direction. The simulated results also showed that the strength of MNAM currents are slightly weaker compared to MNEC simulated currents near the first stagnation point and along the coast of Biddeford pool in the south of the bay. Yet, able to capture the strong flow field near Camp Ellis point that caused significant inundation in that area. Conversely, the strength of the currents in the northern marshy areas of the Saco Bay are comparable between the MNEC and MNAM simulation results. A spatial [6] comparison between the MNAM and MNEC simulated currents during the passage of powerful storm (WS-III) in Saco Bay has been reported in the previous study.

### *3.3 Sensitivity Experiments*

The shallow areas at the northern head of the Saco Bay are predominated by extensive marshland and sand-clogged channels. These areas are likely to induce non-linear over-tide generation. The principle cause for this non-linear process are marshland (which act as intertidal storage) and bottom friction. In order to accurately predict the storm-induced inundation, it is important to understand the influence of these intertidal storage and bottom friction on predicted flooding in these areas of the bay. So, we have performed different sensitivity experiments to assess their effects during the passage of WS-I by varying these parameters.

Sensitivity experiments are conducted based on thoroughly validated MNEC simulation products which is considered here as control run (CR) to perform these experiments. In the first experiment (Exp-1), the marshland elevation was increased by 1 m (Fig. 8c and 8d) and in the second experiment (Exp-2), the marshland elevation was further increased to 2 m (Fig. 8e and 8f) compared to CR. In the third experiment (Exp-3), the marshland elevation was decreased by 1m (Fig. 8g and 8h) from the CR and in the fourth experiment (Exp-4), the bottom friction was increased to 5 times compared to the CR (Fig. 8i and 8j). During the peak of the storm surge, for each experiment, deviation in the flow pattern from the CR was calculated for the whole domain with a special emphasis on the north and south of

Saco Bay to determine the areas that can be affected due to the variation in these parameters. From the illustration (Fig. 8), it is revealed that increasing the intertidal storage even by 2 times ensure not much variation in the flow pattern in the southern bay except in the marshy areas of Biddeford Pool and Goosefare Brook (location shown in Fig. 1b). However, perceptible disparity in the spatial flow pattern has been observed in Exp-1 in most of the areas of the northern Saco Bay including the marshy areas of Pine Point and Scarborough. Therefore, it is evident that the flow dynamics are typically affected by increasing the marshland elevation in the northern areas of the Saco Bay. Conversely, decreasing the marshland elevation hardly effected the overall bay scale flow dynamics except in the Biddeford Pool areas. On the other hand, increasing the domain's friction showed strong effect on the bay scale circulation. From the results, it is revealed that increasing the marshland elevation, a sequential decrease in the rate of water level is observed at Camp Ellis, Biddeford Pool and Pine Point when compared to the control run. Increasing the domain friction in Exp-4 caused tidal asymmetry and impacted the strong flow field areas of the bay. In general, the sensitivity study revealed that the lateral flooding was not much affected as floodward pressure gradient is decreased leading to less surge in flood currents. Storm-induced inundation is not much apparent in Exp-1 and Exp-2 as compared to MNEC.

## 4. Conclusions

Nowadays, storm surge inundation models are getting more attention in coastal communities for assisting in emergency and rapid response activities due to changes in sea level rise, storm intensity and frequency. Therefore, we developed for the first time a unique high-resolution inundation modeling system for the Saco-Casco Bays to accurately predict the storm surges in ungauged areas of the bay. The inundation model well captured the peak tidal height for the five typical winter storms of 2014-2015. The model derived spatial inundation map accurately represented the timing of the inundation and mapped the flood risk areas of the bay. The thorough validation of the model with the NOAA's observed values and real-time CINAR storm buoy data suggests that the inundation model is a useful tool for predicting the coastal flooding along the northeast coast of U.S. However, the methodology can be used globally to predict the inundation in similar coastal areas where data is limited and tide gauge station is unavailable.

Further, the model runs were driven by two different sets of meteorological forcing which determined the effect of spatial resolution, wind velocity on the estimation of peak tidal height during the passage of WS. These model-model comparisons identified the bias in tidal prediction during the peak of storm-induced tide. Indeed, uncertainties in wind speed and direction [15, 16] are likely to cause peak surge underestimation and phase difference. Even though previous study [8] suggests that implementation of high-resolution model grid can aid with better predictive skill, yet it is still important to drive these modeling framework with high-resolution forcing field (1 km × 1 km) in future which could play important role in explaining the differences in positive extremes.

In all the storm surge scenarios, southward wind-driven coastal current flowing towards Biddeford Pool, Pine Point and Camp Ellis forms a small-scale eddy which causes significant inundation however the strength of the currents varies for different storm surge scenarios and depends on storm intensity. In future, inclusion of wave-current interface in the inundation model would be tested to better the predictive skill. Moreover, sensitivity experiments based on varying parameters of marshland elevation and bottom friction determined the influence of intertidal storage on the predicted flooding. It is also important to note that in future any change in

marshland elevation will not only alter the velocities of bay scale currents but will also have an effect on predicted flooding. Overall, the study demonstrates the reasonable capability of the inundation model to provide guidance and information in real-time for multiple simultaneous coastal flooding phenomenon.

## References


[1] Bernier, N. B., and Thompson, K. R. (2006). "Predicting the Frequency of Storm Surges and Extreme Sea Levels in the Northwest Atlantic." *Journal of Geophysical Research: Oceans* 111: C10009.

[2] Narayan, S., Beck, M. W., Reguero, B. G., Losada, I. J., van Wesenbeeck, B., and Pontee, N. et al.(2016). "The Effectiveness, Costs and Coastal Protection Benefits of Natural and Nature-Based Defences." *PLoS ONE* 11: e0154735.

[3] Hallegatte, S., Green, C., Nicholls, R. J., and Corfee-Morlot, J.(2013). "Future Flood Losses in Major Coastal Cities." *Nature Climate Change* 3: 802-806.

[4] Harris, D. L. (1963). "Characteristics of the Hurricane Storm Surge." *U.S. Weather Bureau Technical Paper* 48: 139.

[5] Slovinsky, P. A., and Dickson, S. M. (2007). "State of Maine's Beaches in 2007." *Maine Geological Survey Open-File* 07-99.

[6] Deb, S., and Xue, H. (2017). "Storm Surge Modelling of Saco-Casco Bays: A FVCOM Based Study on Winter Storm Juno." In: *Proceeding of IEEE Xplore of Geoscience and Remote Sensing Symposium*, pp. 3595-3598.

[7] Chen, C., Beardsley, R. C., Luettich, R. A., Westerink, J. J., Wang, H., Perrie, W., and Toulany, B. (2013). "Extratropical Storm Inundation Testbed: Intermodel Comparisons in Scituate, Massachusetts." *Journal of Geophysical Research: Oceans* 118: 5054-5073.

[8] Beardsley, R. C., Chen, C., and Xu, Q. (2013). "Coastal Flooding in Scituate (MA): A FVCOM Study of the 27 December 2010 Nor'easter." *Journal of Geophysical Research: Oceans* 118: 6030-6045.

[9] Chen, C., Liu, H., and Beardsley, R. C. (2003). "An Unstructured Grid, Finite-Volume, Three-Dimensional, Primitive Equations Ocean Model: Application to Coastal Ocean and Estuaries." *Journal of Atmospheric and Oceanic Technology* 20: 159-186.

[10] Smagorinsky, J. (1963). "General Circulation Experiments With the Primitive Equations: I. the Basic Experiment." *Monthly Weather Review* 91: 99-164.

[11] Mellor, G. L., and Yamada, T. (1982). "Development of a Turbulence Closure Model for Geophysical Fluid Problems", *Reviews of Geophysics and Space Physics* 20: 851-875.

[12] Kobayashi, M. H., Pereira, J. M., and Pereira, J. C. (1999). "A Conservative Finite-Volume Second-Order-Accurate Projection Method on Hybrid Unstructured Grids." *Journal of Computational Physics* 150: 40-75.

[13] Lim, E., Taylor, L. A., Eakins, B. W., Carignan, K. S., Warnken, R. R., and Medley, P. R. (2009). "Digital Elevation Model of Portland, Maine: Procedures, Data Sources, and Analysis." National Oceanic and Atmospheric Administration Technical Memorandum NESDIS NGDC-30, Dept. of Commerce, Boulder, CO, U.S. 29.

[14] Large, W. G., and Pond, S. (1981). "Open Ocean Momentum Flux Measurements in Moderate to Strong Winds", *Journal of Physical Oceanography* 11: 324-336.

[15] Deb, S., Xue, H., and Rao, S. (2020). "Storm Surge Inundation Modelling of Five Winter Storms in Saco-Casco Bays: A FVCOM Based Numerical Study." In: *Proceeding of IEEE Xplore of Geoscience and Remote Sensing Symposium*, pp. 5745-5748.

[16] Koračin, D., Dorman, C. E., and Dever, E. P. (2004). "Coastal Perturbations of Marine-Layer Winds, Wind Stress, and Wind Stress Curl Along California and Baja California in June 1999." *Journal of Physical Oceanography* 34: 1152-1173.